

Supplementary Information for “Quantitative rationalization of unexpectedly moderate water wettability on poly (vinyl alcohol) surfaces: Thermodynamic Evaluation and Prediction of Surface Hydrogen Bonding”

Zhuohuan Guo, Zhuoyuan Ma* and Dayang Wang*

State Key Laboratory for Inorganic Synthesis and Preparative Chemistry, College of Chemistry, Jilin University, 130012, Changchun, China

* Corresponding authors. E-mail: wangdayang@jlu.edu.cn, mzyjlu@163.com

Table of Contents:

1. The original SFG spectra of as-prepared $L_PVA_2^{140}$ thin films before and after 80 cycles of abrasion (Figure S1).
2. The original UV-Vis spectra (Figure S2, Figure S8).
3. The original AFM images (Figure S3).
4. The original XPS spectra (Figure S4).
5. The original ATR-FTIR spectra (Figure S5, Figure S6, Figure S9).
6. The original SEM images (Figure S7).
7. Summary of the fitting parameters of ATR-FTIR spectra on $L_PVA_2^T$, $H_PVA_2^{80}$, $L_PVA_7^{RT}$ and $M_PVA_G^{RT}$ thin films (Table S1).
8. Bootstrapping Validation of γ_t^{s,p^*} and γ_g^{s,p^*} values.

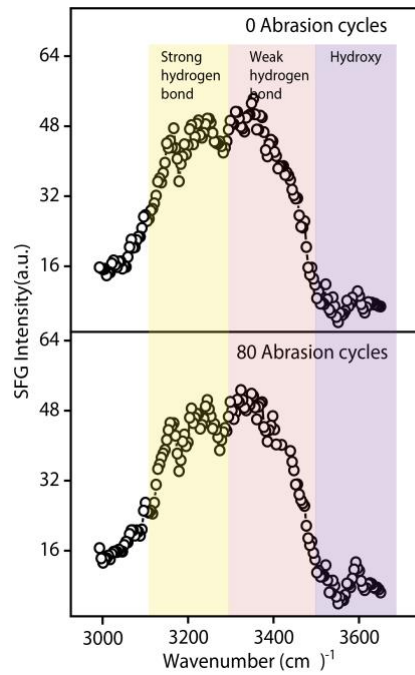


Figure S1. SFG spectra of as-prepared $L_PVA_2^{140}$ thin films before and after 80 cycles of abrasion.

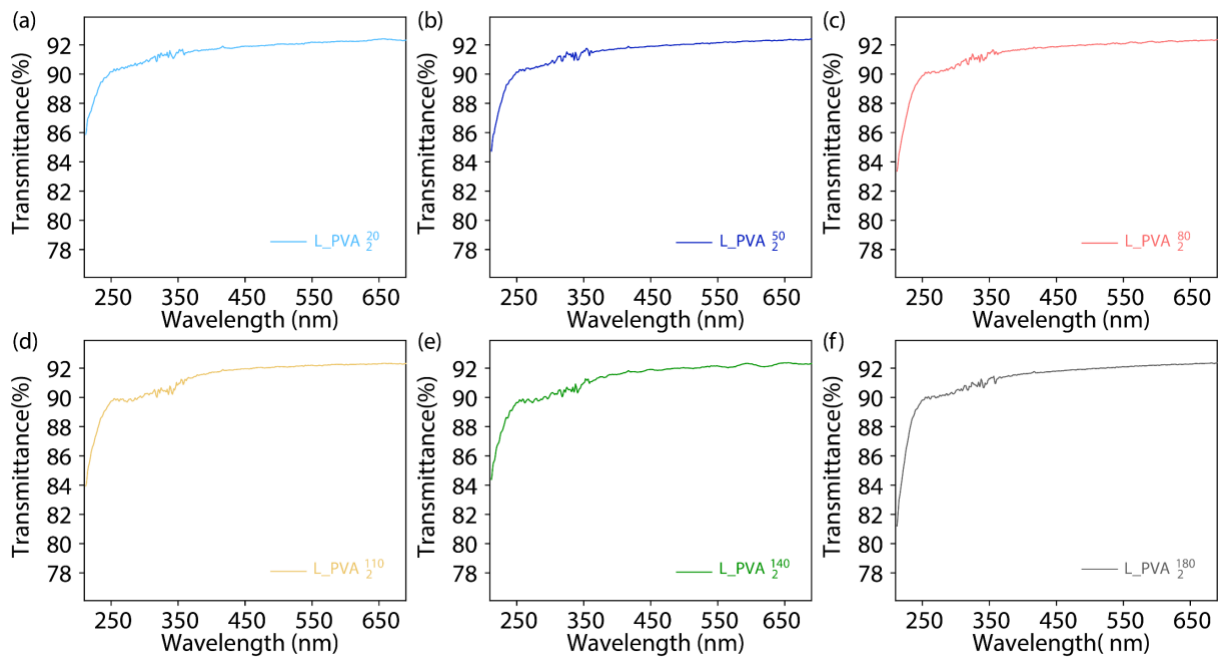


Figure S2. (a-f) UV-Vis spectra of as-prepared $L_PVA_2^{20}$, $L_PVA_2^{50}$, $L_PVA_2^{80}$, $L_PVA_2^{110}$, $L_PVA_2^{140}$ and $L_PVA_2^{180}$ thin films in the wavelength range of 200-700 nm, respectively.

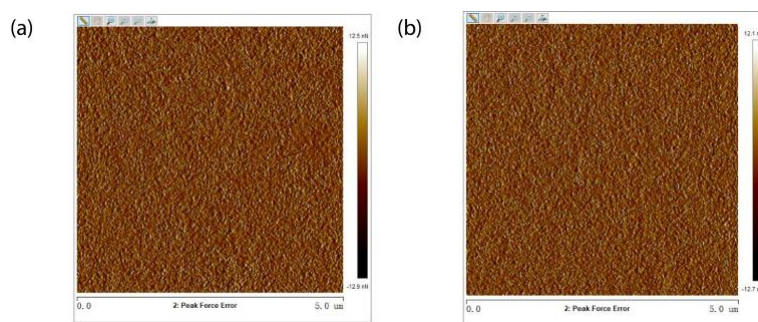


Figure S3. AFM images of as-prepared L_PVA₂²⁰ (a) and L_PVA₂¹⁸⁰ (b) thin films.

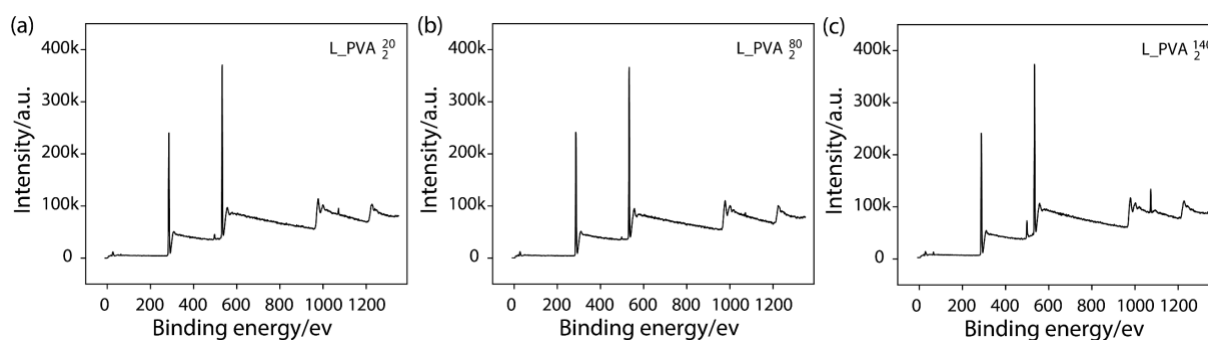


Figure S4. High-resolution XPS spectra of the survey signals of L_PVA₂²⁰ (a), L_PVA₂⁸⁰ (b), and L_PVA₂¹⁴⁰ thin films (c).

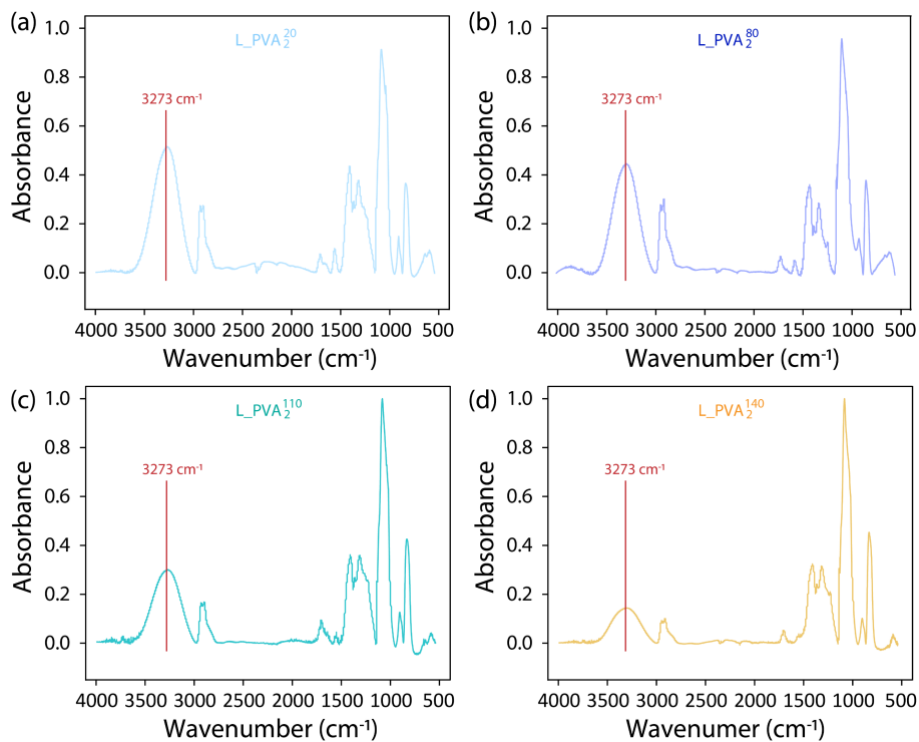


Figure S5. (a-d) ATR-FTIR spectra of as-prepared L_PVA₂²⁰, L_PVA₂⁸⁰, L_PVA₂¹¹⁰, and L_PVA₂¹⁴⁰ thin films in the range of 4000-400 cm⁻¹, respectively.

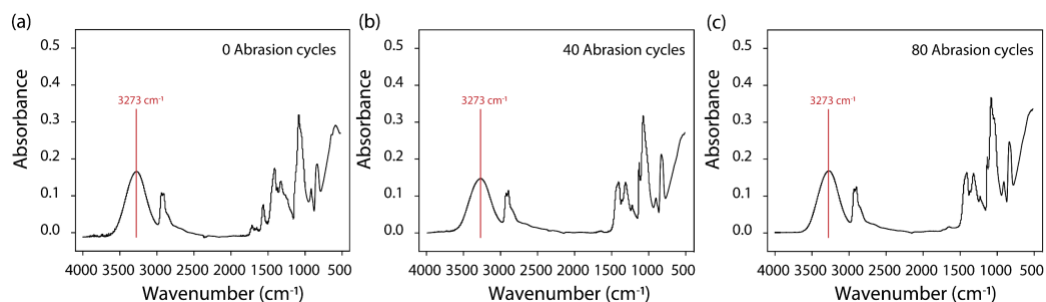


Figure S6. (a-c) ATR-FTIR spectra of as-prepared $L_PVA_2^{140}$ thin films after their surfaces are subjected to 0, 40 and 80 cycles of abrasion, respectively.

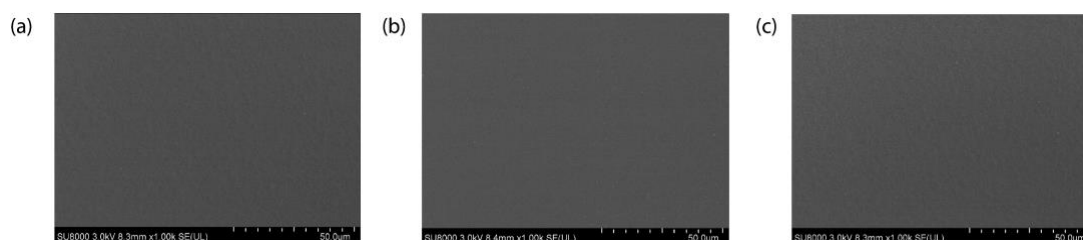


Figure S7. (a-c) SEM images of as-prepared $H_PVA_2^{80}$, $L_PVA_7^{RT}$, and $M_PVA_G^{RT}$ films, respectively.

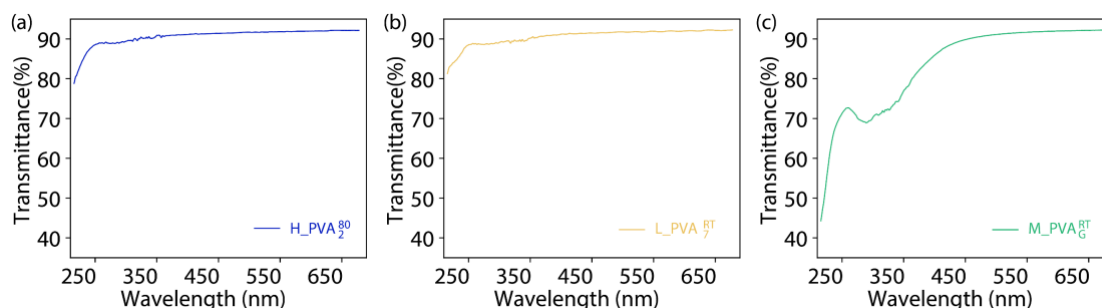


Figure S8. (a-c) UV-Vis spectra of as-prepared $H_PVA_2^{80}$, $L_PVA_7^{RT}$, and $M_PVA_G^{RT}$ films in the wavelength range of 200-700 nm, respectively.

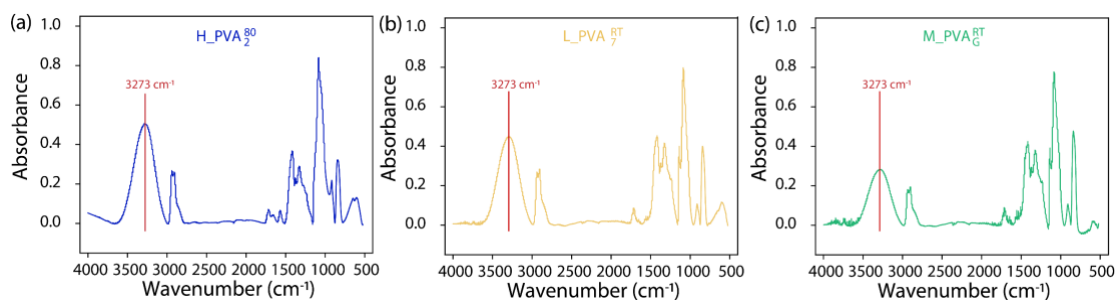


Figure S9. (a-c) ATR-FTIR spectra of $H_PVA_2^{80}$, $L_PVA_7^{RT}$, and $M_PVA_G^{RT}$ films in the range of 4000-400 cm^{-1} , respectively.

Table S1. Summary of the fitting parameters of ATR-FTIR spectra on $L_PVA_2^T$, $H_PVA_2^{80}$, $L_PVA_7^{RT}$ and $M_PVA_G^{RT}$ thin films.

| $L_PVA_2^T$ | OH_t group | | | | OH_g group | | | | R^2 |
|------------------|----------------|-----------------|-----------|-----------------|----------------|-----------------|-----------|-----------------|--------|
| | peak position | Standard errors | peak area | Standard errors | peak position | Standard errors | peak area | Standard errors | |
| $L_PVA_2^{20}$ | 3222 cm^{-1} | 2.4 cm^{-1} | 59.5 | 3.0 | 3356 cm^{-1} | 3.3 cm^{-1} | 41.7 | 3.0 | 0.9937 |
| $L_PVA_2^{80}$ | 3222 cm^{-1} | 1.9 cm^{-1} | 50.5 | 1.9 | 3356 cm^{-1} | 2.2 cm^{-1} | 39.6 | 1.9 | 0.9981 |
| $L_PVA_2^{110}$ | 3222 cm^{-1} | 2.3 cm^{-1} | 37.1 | 1.5 | 3356 cm^{-1} | 2.7 cm^{-1} | 30.0 | 1.5 | 0.9951 |
| $L_PVA_2^{140}$ | 3222 cm^{-1} | 2.0 cm^{-1} | 22.7 | 0.6 | 3356 cm^{-1} | 2.2 cm^{-1} | 42.5 | 0.6 | 0.9959 |
| $H_PVA_2^{80}$ | 3222 cm^{-1} | 2.6 cm^{-1} | 56.5 | 3.8 | 3356 cm^{-1} | 3.0 cm^{-1} | 54.0 | 4.6 | 0.9962 |
| $L_PVA_7^{RT}$ | 3222 cm^{-1} | 5.0 cm^{-1} | 49.8 | 4.7 | 3356 cm^{-1} | 4.0 cm^{-1} | 46.6 | 4.8 | 0.9953 |
| $M_PVA_G^{RT}$ | 3222 cm^{-1} | 2.7 cm^{-1} | 28.5 | 3.7 | 3356 cm^{-1} | 3.5 cm^{-1} | 24.7 | 2.7 | 0.9970 |

Bootstrapping Validation of γ_t^{s,p^*} and γ_g^{s,p^*} values.

Based on the determination method for γ_t^{s,p^*} and γ_g^{s,p^*} values reported in Section 3.3, Line 24, and the data listed in Table 1 (at least three sets), we applied the multivariable linear regression model in Origin to fit Equation 13 and obtained the following values that satisfy the condition: $0 \text{ mN/m} < \gamma_t^{s,p^*}$ and $\gamma_g^{s,p^*} < 50 \text{ mN/m}$:

$$\text{For } \gamma_t^{s,p^*}: (x_1 = 6.2 \text{ mN/m}, x_2 = 8.4 \text{ mN/m}, x_3 = 8.0 \text{ mN/m})$$

$$\text{For } \gamma_g^{s,p^*}: (x_1 = 9.0 \text{ mN/m}, x_2 = 8.5 \text{ mN/m}, x_3 = 9.8 \text{ mN/m})$$

The 95% confidence intervals for γ_t^{s,p^*} and γ_g^{s,p^*} were calculated using Equation (13), resulting in the following: γ_t^{s,p^*} 95% CI: $7.5 \pm 1.5 \text{ mN/m}$; γ_g^{s,p^*} 95% CI: $9.1 \pm 1.2 \text{ mN/m}$. The confidence interval formula is described as follows:

$$CI = \bar{x} \pm t \times \frac{SD}{\sqrt{n}} \quad (S1)$$

where \bar{x} is the sample mean, t is the critical value from the t-distribution (2.3534), SD is the standard deviation, and n is the sample size.